Acta Cryst B
STRUCTURAL SCIENCE
CRYSTAL ENGINEERING
MATERIALS
ISSN 2052-5206

Accurate hydrogen parameters for the amino acid L-leucine

HPSTAR
256-2016

Jack Binns,[a,b]*‡ Simon Parsons[b] and Garry J. McIntyre[a]

[a]Australian Nuclear Science and Technology Organisation, New Illawarra Road, Lucas Heights NSW 2234, Australia, and [b]EaStCHEM School of Chemistry and Centre for Science at Extreme Conditions, The University of Edinburgh, The King's Buildings, West Mains Road, Edinburgh EH9 3FJ, Scotland. *Correspondence e-mail: jack.binns@hpstar.ac.cn

Received 13 July 2016
Accepted 5 October 2016

Edited by F. P. A. Fabbiani, University of Göttingen, Germany

‡ Current affiliation: Center for High Pressure Science & Technology Advanced Research, 1690 Cailun Road, Pudong, Shanghai 201203, People's Republic of China

Keywords: amino acids; neutron diffraction; Laue diffraction; crystal packing.

CCDC references: 1508363; 1508364

Supporting information: this article has supporting information at journals.iucr.org/b

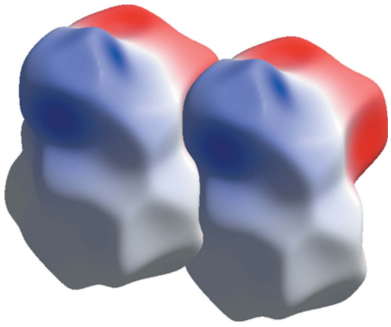

The structure of the primary amino acid L-leucine has been determined for the first time by neutron diffraction. This was made possible by the use of modern neutron Laue diffraction to overcome the previously prohibitive effects of crystal size and quality. The packing of the structure into hydrophobic and hydrophilic layers is explained by the intermolecular interaction energies calculated using the PIXEL method. Variable-temperature data collections confirmed the absence of phase transitions between 120 and 300 K in the single-crystal form.

1. Introduction

The advantages of neutron diffraction for providing accurate geometric parameters for amino acids and other molecular materials are well known, and include the strong and contrasting scattering lengths of hydrogen and deuterium, and the absence of form-factor fall off with scattering angle (Niimura & Bau, 2008; McIntyre, 2014; Görbitz, 2015). Accurate geometric parameters for H atoms are especially important as structures derived from X-ray studies suffer from severe systematic errors as a result of aspherical electron-density distributions about covalently bonded hydrogen.

Overall, a total of 16 of the 20 naturally occurring amino acids have been subject to structure determination by neutron diffraction. In the early 1970s Hamilton and colleagues at Brookhaven National Laboratory refined the structures, including the all-important H atoms, of 13 of the 20 naturally occurring amino acids in an ambitious series of single-crystal neutron diffraction studies (see references below). Three further structures came from experiments at the Indian Atomic Energy Laboratory, Trombay, to create a library of accurate and complete structures.

Of the amino acids with electrically charged side-chains, structures have been obtained for L-arginine (Lehmann *et al.*, 1973), L-histidine (Lehmann *et al.*, 1972*a*), L-lysine (Koetzle *et al.*, 1972) and L-glutamic acid (Lehmann *et al.*, 1972*b*; Lehmann & Nunes, 1980) in the enantiopure form, while aspartic acid was determined in the racemic DL-aspartic acid form (Sequeira *et al.*, 1989). Of the polar uncharged amino acids neutron-diffraction-derived structures have been determined for L-serine (Frey *et al.*, 1973), L-threonine (Ramanadham *et al.*, 1973*b*), L-asparagine (Verbist *et al.*, 1972; Ramanadham *et al.*, 1972; Weisinger-Lewin *et al.*, 1989) and L-glutamine (Koetzle *et al.*, 1973). Of the hydrophobic side-chain amino acids, structures have been determined by neutron diffraction for L-alanine (Lehmann *et al.*, 1972*c*; Wilson *et al.*,

2005), L-valine (Koetzle, 1974), L-phenylalanine (Al-Karaghouli & Koetzle, 1975), L-tyrosine (Frey, 1973) and L-tryptophan (Andrews *et al.*, 1974). Of the remaining amino acids, structures have been determined for L-cysteine (Ramanadham *et al.*, 1973*a*) and L-glycine in both α (Jönsson & Kvick, 1972) and γ polymorphs (Kvick *et al.*, 1980).

Amino-acid structural parameters derived from neutron diffraction have found extensive application as constraints and restraints in macromolecular refinements, and many of the entries above are still the preferred standards today and remain heavily cited in the literature. These publications have a mean number of citations of 83 overall, and 20 in the last 5 years. For example, neutron structures are used for restraints applied to C, N and O positions in the program suite *PROTIN*/*PROLSQ* (Konnert & Hendrickson, 1980), and are particularly valuable when applied to the joint refinement of X-ray and neutron data (Wlodawer & Hendrickson, 1982). They are also used for validation of refined protein structures. Hydrogen constitutes *ca* 50% of the atoms in macromolecules (Myles, 2006), and it is essential to include it in refinement models. Although the derived X—H restraints need to be shortened for X-ray protein refinements, the neutron library gives considerably more accurate bond directionality than an X-ray-based library (Konnert, 1976; Wlodawer & Hendrickson, 1982; Hendrickson & Konnert, 1981; Teeter & Kossiakoff, 1983; Niimura *et al.*, 1997). Of course, the derived X—H restraints apply without adjustment to refinement of protein structures based on neutron data, which is growing in importance thanks to experimental improvements of the type described below (Munshi *et al.*, 2012).

The neutron structure of L-leucine has not been reported. The Brookhaven and Trombay studies required single crystals with volumes of 10 mm^3 or more, and for the three amino acids, L-leucine, L-isoleucine and L-methionine, only crystals of volumes suitable for X-ray diffraction could be grown. L-Leucine proved to be particularly troublesome, but methods for growing crystals of volumes of 0.1 mm^3 are now known (Görbitz & Dalhus, 1996*b*). The use of Laue (white beam) diffraction coupled with advances in neutron image-plate technology has increased the range of applicability of neutron crystallography (Cole *et al.*, 2001; McIntyre *et al.*, 2006), and the LADI and VIVALDI instruments at the ILL pioneered the application of this technique to macromolecular and small-molecule crystallography, respectively (Cipriani *et al.*, 1996; Wilkinson *et al.*, 2002). The technique is eminently suitable for crystals with volumes of 0.1 mm^3 (McIntyre *et al.*, 2006; Aznavour *et al.*, 2008; Edwards, 2011). Here we report the neutron-diffraction-derived structures of L-leucine at 120 K and room temperature as determined using the KOALA Laue diffractometer at ANSTO.

The structure of L-leucine was first determined by Harding & Howieson (1976) with subsequent redeterminations by Coll *et al.* (1986) and most recently Görbitz & Dalhus (1996*b*) as part of a series of redeterminations of amino-acid structures. When studied using single-crystal methods, the room-temperature phase of L-leucine persists to 120 K; the structure at this temperature is monoclinic, $P2_1$, a = 9.562 (2), b = 5.301 (1), c = 14.519 (3) Å, β = 94.20 (2)° (Görbitz & Dalhus, 1996*b*).

By contrast, when studied by powder diffraction L-leucine has been reported to undergo three phase transitions at 150, 275 and 353 K (Façanha Filho *et al.*, 2011). A combination of calorimetric and X-ray powder diffraction data was used to identify two transitions at T_1 = 150 K and T_2 = 275 K. Additional peaks in the X-ray powder diffraction data were taken as an indication of a doubled a unit-cell length, however, a limited 2θ range precluded a Rietveld analysis (Rietveld, 1969; Façanha Filho *et al.*, 2011). The unit-cell dimensions derived from Le Bail fitting (Le Bail *et al.*, 1988) exhibit two sharp discontinuities in the β angle. Analysis of the systematic absences was ambiguous, but the requirement for enantiopurity implied either $P2$ or $P2_1$. As noted by Façanha Filho *et al.* (2011), there is a need for additional high-resolution diffraction data to characterize the transitions fully.

2. Crystallization, data collection and refinement

A single colourless plate of 2 × 0.5 × 0.2 mm of L-leucine (Aldrich) was grown from a warm (*ca* 323 K) concentrated aqueous solution which was allowed to cool to room temperature (Harding & Howieson, 1976; Görbitz & Dalhus, 1996*b*).

Neutron diffraction data were collected on the KOALA quasi-Laue diffractometer, ANSTO, at 120 and 300 K. Data were collected in two orientations of the crystal relative to the single (vertical) rotation axis of the instrument in order to optimize completeness. The exposure time was 2 h per pattern at both temperatures.

At 120 K, nine Laue patterns were collected in each crystal setting giving a total of 18 patterns. Patterns were related by a 20° rotation about the vertical axis in the range $-90 < \varphi < 90°$.

At 300 K, 11 patterns were collected in one setting in a φ range of $-90 < \varphi < 90°$ and $-80 < \varphi < 40°$ with $\Delta\varphi = 20°$, a further 17 patterns were collected in the second setting over a φ range of $-90 < \varphi < 90°$ with $\Delta\varphi = 10°$, giving a total of 28 patterns.

Short collections (10 min each) were also carried out during the heating and cooling process to check for signs of additional Bragg peaks that would be diagnostic of phase transitions. Cooling the sample crystal to 120 K led to the appearance of splitting in the Laue spots. The degree of splitting was not uniform over the detector surface indicting that the splitting arises from a macroscopic movement of layers making up the crystal, rather than changes in atomic structure. Furthermore, subsequent heating of the sample back to room temperature led to no significant changes in the shape of the Laue diffraction spots. Structure factors could nevertheless be extracted from these patterns, although the overall quality of the data at 120 K is a little lower than for those at room temperature.

The Laue diffraction patterns were indexed and processed using the program *LaueG* (Piltz, 2016). Reflection intensities were integrated with a modified two-dimensional version of the algorithm formulated by Wilkinson *et al.* (1988) and Prince

Table 1
Crystal data and details of the structure determination of L-leucine at 300 and 120 K.

Values in italics are derived from X-ray diffraction measurements.

	300 K	120 K
Crystal data		
Chemical formula	$C_6H_{13}NO_2$	$C_6H_{13}NO_2$
M_r	131.17	131.17
Crystal system, space group	Monoclinic, $P2_1$	Monoclinic, $P2_1$
Temperature (K)	300	120
a, b, c (Å)	9.606 (3), 5.324 (7), 14.666 (2)†	9.562 (2), 5.301 (1), 14.519 (3)‡
β (°)	94.06 (3)†	94.20 (2)‡
V (Å^3)	748.2 (10)†	734.0 (3)‡
Z	4	4
Radiation type	Neutron, λ = 0.80–1.7 Å	Neutron, λ = 0.80–1.7 Å
Crystal size (mm)	2 × 0.5 × 0.2	2 × 0.5 × 0.2
Data collection		
Diffractometer	KOALA, ANSTO	KOALA, ANSTO
Absorption correction	–	–
No. of measured, independent and observed [$I > 2\sigma(I)$] reflections	24 819, 1648, 1367	21 729, 2430, 1955
R_{int}	0.112	0.156
$(\sin\theta/\lambda)_{max}$ (Å^{-1})	1.185	1.184
Refinement		
$R[F^2 > 2\sigma(F^2)]$, $wR(F^2)$, S	0.058, 0.134, 1.10	0.079, 0.171, 1.14
No. of reflections	1647	2429
No. of parameters	397	397
No. of restraints	361	361
H-atom treatment	All H-atom parameters refined	All H-atom parameters refined
$\Delta\rho_{max}$, $\Delta\rho_{min}$ (e Å^{-3})	0.55, −0.63	1.29, −1.40

† Coll *et al.* (1986). ‡ Görbitz & Dalhus (1996*b*).

et al. (1997). Resolution limits were determined based on the shortest d-spacing at which 5% of reflections had $I/\sigma(I) > 5$. The data were empirically normalized to a single common incident wavelength using the program *Laue*4 (Piltz, 2011), by comparison of repeat observations and equivalent reflections with wavelengths within the range λ = 0.80–1.7 Å; reflections outside this range were too weak or had too few repeat measurements or equivalents to be able to determine the normalization curve with confidence. Absorption or extinction corrections were deemed unnecessary on account of the small sample size.

Refinement of the crystal structures was carried out against $|F^2|$ with the *SHELXL* refinement package (Sheldrick, 2015) using least-squares minimization with initial atomic coordinates provided by Görbitz & Dalhus (1996*b*). Crystal and refinement data are listed in Table 1. Unit-cell dimensions for the room temperature and 120 K data-sets were therefore taken from corresponding X-ray diffraction studies (Coll *et al.*, 1986; Görbitz & Dalhus, 1996*b*).

Fig. 1 shows the refined wavelength spectra for data collected at 300 and 120 K, and the nominal instrument spectrum. The shifts in wavelength distribution are negligible; −0.7% for 120 K and +0.3% for 300 K, implying that the unit-cell dimensions provided by the X-ray data of Görbitz & Dalhus (1996*b*) and Coll *et al.* (1986) match our data.

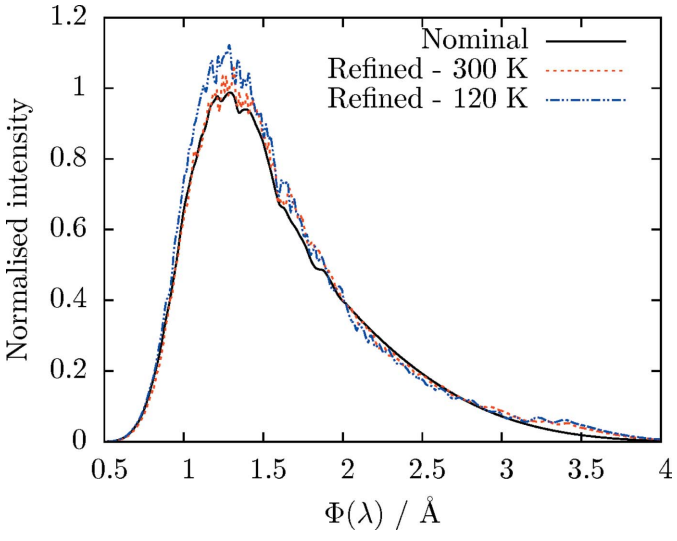

Figure 1
Refined and normalized instrument wavelength spectra for Laue data collected at 120 and 300 K, the nominal spectrum is included for comparison.

Molecular geometries were analysed using *PLATON* (Spek, 2009). Intermolecular interaction energies were calculated using the PIXEL method (Gavezzotti, 2005, 2011). Electron densities were calculated using *GAUSSIAN*09 at the MP2 level of theory with the 6-31G** basis set (Frisch *et al.*, 2009). PIXEL calculations were accomplished with the PixelC module of the CLP package which allows the calculation of dimer and lattice energies.

Hirshfeld surfaces, which enable graphical comparison of molecular interactions for similar configurations, were calculated using *CrystalExplorer* 3.1 (Wolff *et al.*, 2012). The Hirshfeld surface for a given molecule in a given crystal is an isosurface calculated from the ratio of the molecular electron density (the promolecule) over the electron density given by the sum of atoms in the crystal (the procrystal; Turner *et al.*, 2015). Electrostatic potentials were mapped onto these surfaces over the range −0.173 to +0.286 a.u.

3. Structure of L-leucine

3.1. Structure at 120 K

At 120 K the structure of L-leucine was modelled using the unit-cell dimensions determined by Görbitz & Dalhus (1996*b*), $P2_1$, a = 9.562 (2), b = 5.301 (1), c = 14.519 (3) Å, β = 94.20 (2)°. Integration was carried out to a resolution of 0.65 Å. Normalization, including recovery of second-order

Table 2
Selected bond lengths in L-leucine at 120 and 300 K.

	Bond length (Å)			Bond length (Å)	
Bond	120 K	300 K	Bond	120 K	300 K
O1—C1	1.257 (5)	1.256 (5)	C6—H11	1.115 (14)	1.05 (2)
O2—C1	1.244 (6)	1.243 (7)	C6—H12	1.081 (14)	1.03 (2)
N1—C2	1.493 (4)	1.489 (4)	C6—H13	1.076 (16)	1.02 (2)
C1—C2	1.534 (4)	1.536 (4)	N2—H17	1.033 (8)	1.033 (10)
N1—H4	1.046 (8)	1.046 (8)	N2—H15	1.041 (9)	1.031 (10)
N1—H2	1.021 (9)	1.019 (9)	N2—H16	1.065 (8)	1.045 (9)
N1—H3	1.073 (7)	1.061 (8)	C7—C8	1.535 (4)	1.527 (5)
C2—C3	1.541 (4)	1.532 (5)	C8—C9	1.531 (5)	1.523 (6)
C3—C4	1.527 (5)	1.527 (7)	C9—C10	1.535 (7)	1.525 (9)
O3—C7	1.264 (5)	1.254 (5)	C10—C11	1.523 (7)	1.535 (12)
C4—C6	1.529 (6)	1.559 (9)	C10—C12	1.519 (7)	1.522 (11)
C4—C5	1.526 (6)	1.519 (9)	C8—H14	1.097 (9)	1.081 (10)
O4—C7	1.257 (6)	1.244 (7)	C9—H18	1.083 (12)	1.076 (15)
N2—C8	1.490 (4)	1.503 (5)	C9—H19	1.111 (11)	1.108 (15)
C2—H1	1.099 (9)	1.094 (9)	C10—H20	1.075 (15)	1.06 (2)
C3—H5	1.101 (10)	1.080 (12)	C11—H24	1.077 (15)	1.06 (2)
C3—H6	1.107 (10)	1.082 (11)	C11—H25	1.075 (16)	1.03 (3)
C4—H7	1.108 (11)	1.060 (15)	C11—H26	1.078 (16)	0.98 (2)
C5—H10	1.097 (13)	1.05 (2)	C12—H21	1.12 (2)	1.07 (3)
C5—H8	1.083 (12)	1.040 (17)	C12—H22	1.08 (2)	1.02 (4)
C5—H9	1.078 (12)	1.01 (2)	C12—H23	1.11 (2)	1.10 (3)

harmonic reflections, was carried out using a wavelength range of 0.8–1.7 Å giving an R_{merge} value of 0.155 for all 21 729 reflections. Completeness was 79.3% giving a redundancy of 6.1. The harmonic overlap of reflections results in a maximum possible completeness of 83.3% for Laue diffraction (Cruickshank *et al.*, 1987). Final R_1 was 0.0790 [$I > 2\sigma(I)$] and wR_2 was 0.1713 (all data).

The asymmetric unit consists of two L-leucine molecules as shown below in Fig. 2, which will be referred to as *A* [for C1–6] and *B* [for C7–12] after Görbitz & Dalhus (1996*b*). Bond lengths at 120 and 300 K are given in Table 2.

The molecules interact through hydrogen bonds to form layers with isobutyl chains on the upper and lower faces. The layers are of the 'L2' type identified by Görbitz, which *ab initio* calculations suggest contain the most stable interactions (Görbitz, 2015). The layers stack along the [001] direction so that the crystal packing is characterized by hydrophobic and hydrophilic zones alternating along the *c* axis, similar to the arrangement of other hydrophobic amino acids, L-valine, L-methionine and L-isoleucine (Fig. 3; Dalhus & Görbitz, 1996; Görbitz & Dalhus, 1996*a*; Görbitz, 2015). The energy framework based on the results of PIXEL calculations shown in Fig. 4(*a*) demonstrates quantitatively the distribution of strong and weak contacts (Turner *et al.*, 2015); the same picture emerges from an energy vector analysis using the ProcessPIXEL procedure (Bond, 2014). Thick red and green lines linking molecular centroids correspond respectively to hydrogen-bonding contacts of −146 and *ca* −100 kJ mol^{-1}, which form the layers; other hydrogen-bonding interactions are also present, but these all support the two strong contacts depicted in Fig. 4(*a*). The thin blue lines in Fig. 4(*a*) represent contacts of only about −4 kJ mol^{-1} which link the layers together.

A detailed analysis of the intermolecular interaction energies obtained from the PIXEL calculations is presented in Tables 3 and 4. Hydrogen-bond energies fall between −146 and −46 kJ mol^{-1}, the strongest being formed between molecules *A* and *B*. Each L-leucine molecule forms eight hydrogen bonds. Leu-*A* forms three donor contacts through the N1 ammonium group *via* N1—H4···O3, N1—H3···O3^{ii}

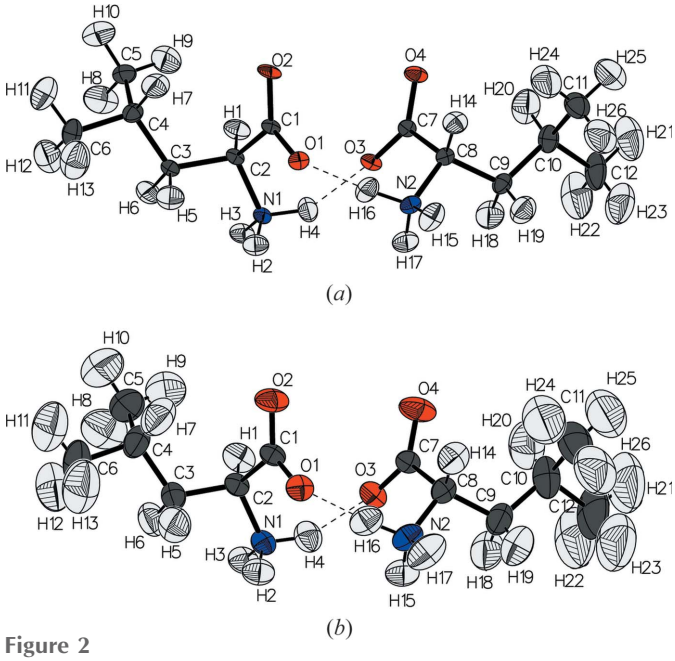

Figure 2
(*a*) Asymmetric unit for L-leucine at 120 K. Ellipsoids are shown at 50% probability; (*b*) asymmetric unit for L-leucine at 300 K. The two hydrogen bonds within the asymmetric unit are shown as dashed lines.

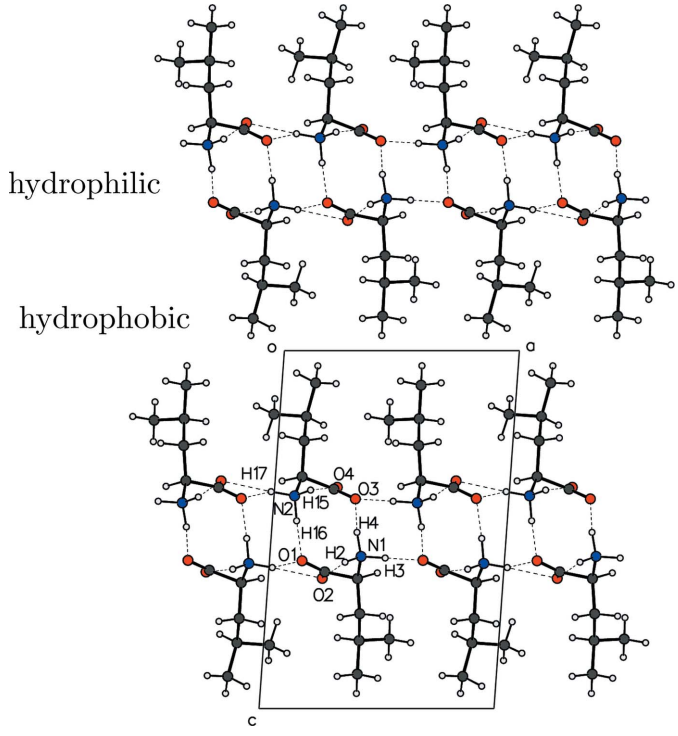

Figure 3
Crystal packing is divided into hydrophilic and hydrophobic layers. Atoms in the asymmetric unit involved in hydrogen bonding are labelled.

Table 3
PIXEL component energies for leu-*A* in L-leucine at 120 K.

Energies are in kJ mol^{-1}.

Distance (Å)	E_{Coul}	E_{Pol}	E_{Disp}	E_{Rep}	E_{Tot}	Symmetry	Notable contacts	Contact distance (Å)	Contact angle (°)	Comment
Hydrophilic layer: interactions with leu-*A* as the central atom										
7.328	−156.2	−76.0	−28.8	115.8	−145.2	$AB[x, y, z]$	N1—H4···O3	1.852 (9)	151.0 (7)	
							O1···H16—N2	1.690 (9)	173.3 (8)	
5.996	−109.6	−32.0	−17.6	45.8	−113.5	$AB[-x, y-\frac{1}{2}, -z+1]$	O2···H17—N2	1.970 (9)	162.2 (9)	[Bifurcation: O1···N2—H17 2.208 (11) 132.1 (8)]
5.030	−128.4	−49.5	−29.1	101.0	−106.0	$AB[-x+1, y+\frac{1}{2}, -z+1]$	N1—H3···O3	1.673 (8)	178.2 (6)	
8.543	−51.0	−6.9	−4.3	1.9	−60.3	$AB[x, y+1, z]$	N1—H4···O4	2.710 (9)	116.60 (6)	NH_3—COO electrostatic
5.301	−39.4	−28.3	−25.2	46.4	−46.5	$AA[x, y-1, z]$	O2···H2—N1	1.886 (9)	170.0 (7)	
5.301	−39.4	−28.3	−25.2	46.4	−46.5	$AA[x, y+1, z]$	N1—H2···O2	1.886 (9)	170.0 (7)	
7.583	31.1	−6.6	−5.3	0.8	20.1	$AA[-x+1, y+\frac{1}{2}, -z+1]$	N1···N1	4.099 (3)		NH_3—NH_3 Repulsion diagonally between red struts
7.583	31.1	−6.6	−5.3	0.8	20.1	$AA[-x+1, y-\frac{1}{2}, -z+1]$	N1···N1	4.099 (3)		NH_3—NH_3 Repulsion diagonally between red struts
5.842	17.5	−6.2	−14.1	11.0	8.1	$AB[-x+1, y-\frac{1}{2}, -z+1]$	C2—H1···O3	3.083 (9)	167.2 (6)	Repulsive psuedo-translation
5.209	10.5	−15.4	−23.1	31.5	3.6	$AB[-x, y+\frac{1}{2}, -z+1]$	O1···H14—C8	2.175 (9)	167.2 (6)	Note overall repulsion
Hydrophobic layer: interactions with leu-*A* as the central atom										
8.331	−1.2	−0.8	−6.3	4.5	−3.8	$AA[-x+1, y-\frac{1}{2}, -z+2]$	C6—H11···H12	2.318 (18)	161.6 (12)	These three molecules form a triangular array above the methyl group based on C6
8.331	−1.2	−0.8	−6.3	4.5	−3.8	$AA[-x+1, y+\frac{1}{2}, -z+2]$	C6—H12···H11	2.318 (18)	128.8 (10)	
8.327	−1.3	−0.5	−4.6	2.8	−3.7	$AB[x, y, z+1]$	C6—H11···H22	2.49 (2)	124.7 (12)	

[(ii) $1-x, y+\frac{1}{2}, 1-z$] and N1—H2···O2^{i} [(i) $x, y+1, z$]. The ammonium group of leu-*B* forms four donor contacts through the N2 amine group: N2—H16···O1 and N2—H15···O4^{1} with N2—H17 forming a bifurcated contact with O1^{ii} and O2^{ii}. The differences in intermolecular energies are determined not by the lengths of the hydrogen bonds but by the relative juxtaposition of and amount of overlap between positively and negatively charged regions of the molecules, illustrated for the strongest and weakest hydrogen-bonding interactions in Figs. 4(*b*) and (*c*).

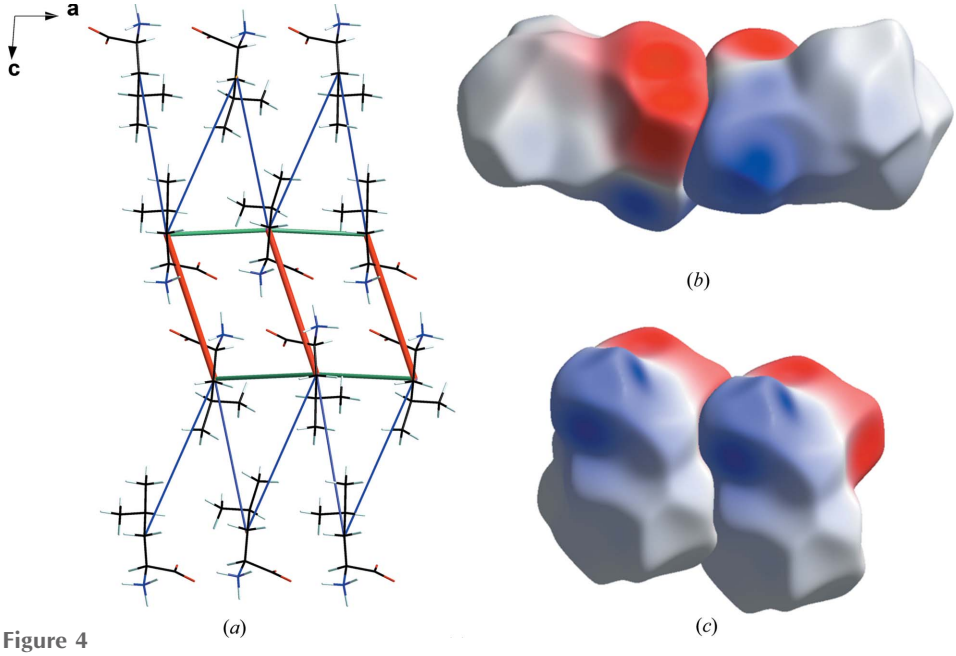

Figure 4
(*a*) Energy framework (Turner *et al.*, 2015) of leucine at 120 K viewed along **b**. The thick coloured lines link the centroids of molecules connected by hydrogen bonds where the red lines correspond to an interaction with total intermolecular energy −145.2 kJ mol^{-1}, and green lines to interactions with energies −113.5 and −106.0 kJ mol^{-1}. The thin blue lines correspond to dispersion interactions with energies between −3 and −4 kJ mol^{-1}. See Tables 3 and 4 for details of the contacts. Hirshfeld surfaces mapped according to electrostatic potential for two hydrogen-bonding interactions. (*b*) N1—H4···O3/O1···H16—N2, which has an energy of −145.2 kJ mol^{-1}. (*c*) N1—H2···O2 which has an energy of −46.5 kJ mol^{-1}. The surfaces are mapped in the range −0.173 a.u. (red) to +0.286 a.u. (blue).

There is one interaction which is also formed between molecules leu-*A* and leu-*B* which, although it is highly stabilizing (−60.3 kJ mol^{-1}), is characterized by quite long interatomic distances, *e.g.* N1- - -O4 measuring 2.710 (9) Å. It is distinguished from the more conventional hydrogen bonds by the overwhelming dominance of the electrostatic component, with only a very small contribution from dispersion, and it is best described as an ionic ammonium-carboxylate interaction. As has been noted in the structures of other amino acids, a number of destabilizing contacts are also present (Gavezzotti, 2002; Volkov & Coppens, 2004; Funnell *et al.*, 2010; Dunitz & Gavezzotti,

Table 4
PIXEL component energies for leu-*B* in L-leucine at 120 K.

Energies are in kJ mol^{-1}.

Distance (Å)	E_{Coul}	E_{Pol}	E_{Disp}	E_{Rep}	E_{Tot}	Symmetry	Notable contacts	Contact distance (Å)	Contact angle (°)	Comment
Hydrophilic layer: interactions with leu-*B* as the central atom										
7.328	−156.2	−76.0	−28.8	115.8	−145.2	$BA[x, y, z]$	N2—H16···O1	1.690 (9)	173.3 (8)	
							O3···H4—N1	1.852 (9)	151.0 (7)	
5.996	−109.6	−32.0	−17.6	45.8	−113.5	$BA[-x, y+\frac{1}{2}, -z+1]$	N2—H17···O2	1.970 (9)	162.2 (9)	[Bifurcation: N2—H17···O1 2.208 (11) 132.1 (8)]
5.030	−128.4	−49.5	−29.1	101.0	−106.0	$BA[-x+1, y-\frac{1}{2}, -z+1]$	O3···H3—N1	1.673 (8)	178.2 (6)	
8.543	−51.0	−6.9	−4.3	1.9	−60.3	$BA[x, y-1, z]$	O4···H4—N1	2.710 (9)	116.60 (6)	NH_3—COO electrostatic
5.301	−38.8	−33.4	−24.4	49.9	−46.7	$BB[x, y+1, z]$	N2—H15···O4	1.836 (9)	166.8 (8)	
5.301	−38.8	−33.4	−24.4	49.9	−46.7	$BB[x, y-1, z]$	O4···H15—N2	1.836 (9)	166.8 (8)	
8.025	17.7	−5.2	−3.7	0.2	9.1	$BB[-x, y+\frac{1}{2}, -z+1]$	N1···N1	4.314 (4)		NH_3—NH_3 Repulsion diagonally between red struts
8.025	17.7	−5.2	−3.7	0.2	9.1	$BB[-x, y-\frac{1}{2}, -z+1]$	N1···N1	4.314 (4)		NH_3—NH_3 Repulsion diagonally between red struts
5.842	17.5	−6.2	−14.1	11.0	8.1	$BA[-x+1, y+\frac{1}{2}, -z+1]$	O3···H1—C2	3.083 (9)	167.2 (6)	Repulsive psuedo-translation
5.209	10.5	−15.4	−23.1	31.5	3.6	$BA[-x, y-\frac{1}{2}, -z+1]$	C8—H14···O1	2.175 (9)	167.2 (6)	Note overall repulsion
Hydrophobic layer: interactions with leu-*B* as the central atom										
7.965	−0.6	−0.4	−5.7	2.6	−4.2	$BB[-x, y-\frac{1}{2}, -z]$	C12—H21···H23	2.678 (20)	123.6 (13)	These three molecules form a triangular array above the methyl group based on C12
							C11—H25···H23	2.668 (19)	126.8 (12)	
7.965	−0.6	−0.4	−5.7	2.6	−4.2	$BB[-x, y+\frac{1}{2}, -z]$	C12—H23···H21	2.678 (20)	165.1 (15)	
							C11—H25···H21	2.668 (19)	115.1 (12)	
8.327	−1.3	−0.5	−4.6	2.8	−3.7	$BA[x, y, z-1]$	C12—H22···H11	2.49 (2)	125.0 (13)	

2012; Moggach *et al.*, 2015). These arise because the strong hydrogen bonds described above position pairs of ammonium groups in relatively close proximity (N···N ∼ 4 Å). Such interactions, which have been described as 'electrostatically compressed', are a feature of ionic and zwitterionic structures (Braga *et al.*, 2002; Dunitz *et al.*, 2013; Moggach *et al.*, 2015). A number of contacts which might have been considered to be stabilizing on the basis of short CH···O distances also turn out to be destabilizing when the total, whole-molecule interaction, is considered.

The PIXEL calculations show that the interactions between layers individually amount to *ca* −4 kJ mol^{-1}. The methyl groups based on C6 and C12 are each positioned in close proximity to three methyl groups in the layers above and below. H···H distances lie between 2.3 and 2.7 Å, but the energy breakdown shows that these are really best considered as whole-molecule dispersion interactions.

3.2. Room-temperature structure

The structure of L-leucine was modelled using the unit-cell dimensions of Coll *et al.* (1986) transformed to the standard setting used by Görbitz & Dalhus, $P2_1$, a = 9.606 (3), b = 5.324 (7), c = 14.666 (2) Å, β = 94.06 (3)°, V = 748.2 (3) Å^3, Z = 4. Patterns collected during heating and cooling showed no additional Bragg peaks indicating no discontinuous changes in unit-cell dimensions, confirming that the reported phase transitions are not present in the single-crystal form of L-leucine.

Integration was carried out to a resolution of 0.75 Å. Normalization, including recovery of second-order harmonic reflections, of all 24 819 reflections gave R_{merge} = 0.112, with outliers rejected at $\Delta I > 10\sigma(I)$. Completeness was 80.1% giving a redundancy of 4.1. Final agreement factors were R_1 = 0.0582 [$I > 2\sigma(I)$] and wR_2 = 0.1341 (all data).

The structure is essentially unchanged from that at 120 K, and again the asymmetric unit consists of two L-leucine molecules as shown in Fig. 2(*b*). Bond lengths are given in Table 2. The hydrogen-bonding pattern at room temperature remains similar to that at 120 K. The four methyl groups in the asymmetric unit show a significant disparity in ADPs; the average U_{eq} values for each group are given in Table 5.

3.3. Effects of temperature

Laue diffraction is not capable of determining unit-cell dimensions absolutely using the observed reflection coordinates, only ratios of *a*:*b*:*c*. It is, however, possible to quantify changes in unit-cell lengths of the order of 1% by observed shifts in the refined instrument spectra produced during the normalization process (Piltz, 2011; see also Fig. 1). The resulting cell-length multiplier coefficient can be applied to obtain more accurate unit-cell lengths. A negative shift in the wavelength distribution implies a positive cell-length multiplier coefficient and *vice versa*.

Calculation of the strain tensor (using the method of Ohashi & Burnham, 1973) using unit-cell dimensions at 300 and 120 K shows the greatest thermal expansion (1.03%) occurs approximately along **c*** (0.243, 0, 0.970), making an angle of 14° with **c**, perpendicular to the layers of the structure. Increased thermal motion, particularly within the opposing methyl groups, causes the expansion along this direction in order to reduce the prevalence of close H···H distances. Thermal expansion is less within the layers themselves: 0.43% along **b** and 0.44% approximately along **a** (0.970, 0, −0.243).

Table 5
Average U_{eq} for methyl H atoms at 120 and 300 K.

		U_{eq}(H) (Å^2)	
Molecule	Carbon atom	120 K	300 K
Leu-*A*	C5	0.051 (3)	0.100 (4)
	C6	0.057 (3)	0.115 (5)
Leu-*B*	C11	0.060 (3)	0.121 (5)
	C12	0.075 (3)	0.154 (6)

The most significant structural change upon cooling to 120 K is the reduction in ADP parameters for the terminal methyl groups, although those of leu-*A* still remain larger than leu-*B*. Clearly the enlarged ADPs at 300 K are due at least partially to thermal motion. The significant reduction in this motion is in agreement with the observation from inelastic neutron scattering that significant motion of the CH_3 groups occurs above 150 K in powder form (Façanha Filho *et al.*, 2011).

Upon cooling to 120 K, U_{eq}(H) values for the methyl group based on C6 in leu-*B* and that based on C5 of leu-*A* are statistically similar. $C6H_3$ remains enlarged, although only by a small margin above 5 e.s.d.s.

The hydrogen-bonding distance between hydrophilic layers remains unchanged (Table 6). However, within each layer the bifurcated N2—H17···O1/2 contact is distorted, moving further away from the ideal bifurcated type. The $N2H_3$ group twists towards O2, creating a more linear contact with H17 [∠N2—H17···O2 increasing from 153.3 (13) to 162.2(9)°], and shortening the contact by −0.140 (13) Å. At the same time the complementary N2—H17···O1 distance increases by +0.047 (7) Å with ∠N2—H17···O1 decreasing from 141.8 (11) to 132.1 (8)°.

In agreement with Görbitz & Dalhus (1996*b*) we observe no changes in diffraction patterns that would suggest the presence of phase transitions in the single-crystal form of L-leucine. The spectroscopic and calorimetric data presented by Façanha Filho *et al.* (2011) show evidence of significant changes within the structure of L-leucine in the powder form, which unfortunately could not be verified with suitable diffraction data. Certainly there is a need for further study of L-leucine in the (deuterated) powder form utilizing high-resolution X-ray or neutron powder diffraction to corroborate the observations of Façanha Filho *et al.* (2011).

4. Conclusions

The structure of the natural amino acid L-leucine has been determined by neutron diffraction for the first time at temperatures of 300 and 120 K. The resulting structures yield geometric parameters with sufficient precision and accuracy for inclusion in restraint libraries of macromolecular structure refinements; the estimated standard deviations on X—H bond lengths range from 0.008–0.03 Å at 300 K and 0.008–0.02 Å at 120 K. Due to the small size or poor quality of L-leucine crystals, the determination of the structure by neutron diffraction has required the application of the modern powerful Laue method.

Table 6
Hydrogen bonds in L-leucine at 300 and 120 K.

	D—H (Å)	H···A (Å)	D···A (Å)	∠D—H···A (°)
300 K				
N1—H2···O2	1.019 (9)	1.881 (10)	2.887 (6)	168.4 (7)
N1—H3···O3	1.061 (8)	1.716 (9)	2.775 (5)	176.1 (8)
N1—H4···O3	1.046 (8)	1.835 (10)	2.817 (5)	155.0 (8)
N2—H15···O4	1.031 (10)	1.835 (11)	2.855 (7)	169.6 (9)
N2—H16···O1	1.045 (9)	1.715 (10)	2.756 (5)	174.5 (9)
N2—H17···O1	1.033 (10)	2.071 (15)	2.952 (5)	141.8 (11)
N2—H17···O2	1.033 (10)	2.110 (10)	3.068 (6)	153.3 (13)
C8—H14···O1	1.081 (10)	2.295 (10)	3.368 (6)	171.2 (7)
120 K				
N1—H2···O2	1.021 (9)	1.886 (9)	2.897 (5)	170.0 (7)
N1—H3···O3	1.073 (7)	1.673 (8)	2.745 (4)	178.2 (6)
N1—H4···O3	1.046 (8)	1.852 (9)	2.812 (5)	151.0 (7)
N2—H15···O4	1.041 (9)	1.836 (9)	2.860 (6)	166.8 (8)
N2—H16···O1	1.065 (8)	1.690 (9)	2.751 (5)	173.3 (8)
N2—H17···O1	1.033 (8)	2.208 (11)	2.999 (5)	132.1 (8)
N2—H17···O2	1.033 (8)	1.970 (9)	2.970 (5)	162.2 (9)
C8—H14···O1	1.097 (9)	2.175 (9)	3.254 (5)	167.2 (6)

Calculation of intermolecular interaction energies reveals a pattern of attractive and repulsive interactions. The energies of hydrogen bonds are not correlated with distance but are instead determined by the disposition of positive and negative regions of electrostatic potential. These calculations also reveal a number of important electrostatic interactions, significantly longer than hydrogen-bond distances which are often assumed to be the most important interaction in the analysis of amino-acid structures. As expected for the single-crystal form, no signs of phase transitions were detected during heating or cooling of the single crystal. Cooling leads to minor unit-cell contraction and significantly reduced motion within the alkyl residue as well as minor rearrangements within the hydrogen-bonding network.

Acknowledgements

We thank the Bragg Institute, ANSTO, for the allocation of neutron beam time under proposals 3880 and 4393. JB wishes to thank EPSRC and the Australian Government for funding.

References

Al-Karaghouli, A. R. & Koetzle, T. F. (1975). *Acta Cryst.* B**31**, 2461–2465.
Andrews, L. C., Farkas, R., Frey, M. N., Lehmann, M. S. & Koetzle, T. F. (1974). Am. Crystallogr. Assoc. Spring Meeting.
Aznavour, K., Yousufuddin, M., Bau, R., McIntyre, G. J., Mason, S. A., Chen, X., Lim, S., Plečnik, C. E., Liu, S., Du, B., Meyers, E. A. & Shore, S. G. (2008). *J. Mol. Struct.* **890**, 277–280.
Bond, A. D. (2014). *J. Appl. Cryst.* **47**, 1777–1780.
Braga, D., Maini, L. & Grepioni, F. (2002). *Chem. Eur. J.* **8**, 1804–1812.
Cipriani, F., Castagna, J. C., Wilkinson, C., Oleinek, P. & Lehmann, M. S. (1996). *J. Neutron Res.* **4**, 79–85.
Cole, J. M., McIntyre, G. J., Lehmann, M. S., Myles, D. A. A., Wilkinson, C. & Howard, J. A. K. (2001). *Acta Cryst.* A**57**, 429–434.

Coll, M., Solans, X., Font-Altaba, M. & Subirana, J. A. (1986). *Acta Cryst.* C**42**, 599–601.

Cruickshank, D. W. J., Helliwell, J. R. & Moffat, K. (1987). *Acta Cryst.* A**43**, 656–674.

Dalhus, B. & Görbitz, C. H. (1996). *Acta Chem. Scand.* **50**, 544–548.

Dunitz, J. D. & Gavezzotti, A. (2012). *J. Phys. Chem. B*, **116**, 6740–6750.

Dunitz, J. D., Gavezzotti, A. & Rizzato, S. (2013). *Cryst. Growth Des.* **14**, 357–366.

Edwards, A. J. (2011). *Aust. J. Chem.* **64**, 869–872.

Façanha Filho, P. F., Jiao, X., Freire, P. T. C., Lima, J. A. Jr, dos Santos, A. O., Henry, P. F., Yokaichiya, F., Kremner, E. & Bordallo, H. N. (2011). *Phys. Chem. Chem. Phys.* **13**, 6576–6583.

Frey, M. N., Koetzle, T. F., Lehmann, M. S. & Hamilton, W. C. (1973). *J. Chem. Phys.* **58**, 2547–2556.

Frey, M. N., Lehmann, M. S., Koetzle, T. F. & Hamilton, W. C. (1973). *Acta Cryst.* B**29**, 876–884.

Frisch, M., Trucks, G., Schlegel, H. B., Scuseria, G., Robb, M., Cheeseman, J., Scalmani, G., Barone, V., Mennucci, B. & Petersson, G. (2009). *GAUSSIAN*09, Revision a.02. Gaussian Inc., Wallingford, CT, USA.

Funnell, N. P., Dawson, A., Francis, D., Lennie, A. R., Marshall, W. G., Moggach, S. A., Warren, J. E. & Parsons, S. (2010). *CrystEngComm*, **12**, 2573–2583.

Gavezzotti, A. (2002). *J. Phys. Chem. B*, **106**, 4145–4154.

Gavezzotti, A. (2005). *Z. Kristallogr.* **220**, 499–510.

Gavezzotti, A. (2011). *New J. Chem.* **35**, 1360–1368.

Görbitz, C. H. (2015). *Crystallogr. Rev.* **21**, 160–212.

Görbitz, C. H. & Dalhus, B. (1996*a*). *Acta Cryst.* C**52**, 1464–1466.

Görbitz, C. H. & Dalhus, B. (1996*b*). *Acta Cryst.* C**52**, 1754–1756.

Harding, M. M. & Howieson, R. M. (1976). *Acta Cryst.* B**32**, 633–634.

Hendrickson, W. A. & Konnert, J. H. (1981). *Biomolecular Structure, Conformation, Function and Evolution.* Oxford: Pergamon Press.

Jönsson, P.-G. & Kvick, Å. (1972). *Acta Cryst.* B**28**, 1827–1833.

Koetzle, T. F., Golic, L., Lehmann, M. S., Verbist, J. J. & Hamilton, W. C. (1974). *J. Chem. Phys.* **60**, 4690–4696.

Koetzle, T. F., Frey, M. N., Lehmann, M. S. & Hamilton, W. C. (1973). *Acta Cryst.* B**29**, 2571–2575.

Koetzle, T. F., Lehmann, M. S., Verbist, J. J. & Hamilton, W. C. (1972). *Acta Cryst.* B**28**, 3207–3214.

Konnert, J. H. (1976). *Acta Cryst.* A**32**, 614–617.

Konnert, J. H. & Hendrickson, W. A. (1980). *Acta Cryst.* A**36**, 344–350.

Kvick, Å., Canning, W. M., Koetzle, T. F. & Williams, G. J. B. (1980). *Acta Cryst.* B**36**, 115–120.

Le Bail, A., Duroy, H. & Fourquet, J. L. (1988). *Mater. Res. Bull.* **23**, 447–452.

Lehmann, M. S., Koetzle, T. F. & Hamilton, W. C. (1972*a*). *Int. J. Pept. Protein Res.* **4**, 229–239.

Lehmann, M. S., Koetzle, T. F. & Hamilton, W. C. (1972*b*). *J. Cryst. Mol. Struct.* **2**, 225–233.

Lehmann, M. S., Koetzle, T. F. & Hamilton, W. C. (1972*c*). *J. Am. Chem. Soc.* **94**, 2657–2660.

Lehmann, M. S. & Nunes, A. C. (1980). *Acta Cryst.* B**36**, 1621–1625.

Lehmann, M. S., Verbist, J. J., Hamilton, W. C. & Koetzle, T. F. (1973). *J. Chem. Soc. Perkin Trans. 2*, pp. 133–137.

McIntyre, G. J. (2014). *Neutron News*, **25**, 19–22.

McIntyre, G. J., Lemée-Cailleau, M.-H. & Wilkinson, C. (2006). *Phys. B Condens. Matter*, **385–386**, 1055–1058.

Moggach, S., Marshall, W. G., Rogers, D. M. & Parsons, S. (2015). *CrystEngComm*, **17**, 5315–5328.

Munshi, P., Chung, S.-L., Blakeley, M. P., Weiss, K. L., Myles, D. A. A. & Meilleur, F. (2012). *Acta Cryst.* D**68**, 35–41.

Myles, D. A. A. (2006). *Curr. Opin. Struct. Biol.* **16**, 630–637.

Niimura, N. & Bau, R. (2008). *Acta Cryst.* A**64**, 12–22.

Niimura, N., Minezaki, Y., Nonaka, T., Castagna, J.-C., Cipriani, F., Høghøj, P., Lehmann, M. S. & Wilkinson, C. (1997). *Nat. Struct. Mol. Biol.* **4**, 909–914.

Ohashi, Y. & Burnham, C. (1973). *Am. Mineral.* **58**, 843–849.

Piltz, R. (2011). *Acta Cryst.* A**67**, C155.

Piltz, R. O. (2016). Personal communication.

Prince, E., Wilkinson, C. & McIntyre, G. J. (1997). *J. Appl. Cryst.* **30**, 133–137.

Ramanadham, M., Sikka, S. K. & Chidambaram, R. (1972). *Acta Cryst.* B**28**, 3000–3005.

Ramanadham, M., Sikka, S. K. & Chidambaram, R. (1973*a*). *Acta Cryst.* B**29**, 1167–1170.

Ramanadham, M., Sikka, S. K. & Chidambaram, R. (1973*b*). *Pramana*, **1**, 247–259.

Rietveld, H. M. (1969). *J. Appl. Cryst.* **2**, 65–71.

Sequeira, A., Rajagopal, H. & Ramanadham, M. (1989). *Acta Cryst.* C**45**, 906–908.

Sheldrick, G. M. (2015). *Acta Cryst.* C**71**, 3–8.

Spek, A. L. (2009). *Acta Cryst.* D**65**, 148–155.

Teeter, M. M. & Kossiakoff, A. (1983). *Neutrons in Biology*, edited by B. Schoenborn, pp. 335–348. New York: Plenum Press.

Turner, M. J., Thomas, S. P., Shi, M. W., Jayatilaka, D. & Spackman, M. A. (2015). *Chem. Commun.* **51**, 3735–3738.

Verbist, J. J., Lehmann, M. S., Koetzle, T. F. & Hamilton, W. C. (1972). *Acta Cryst.* B**28**, 3006–3013.

Volkov, A. & Coppens, P. (2004). *J. Comput. Chem.* **25**, 921–934.

Weisinger-Lewin, Y., Frolow, F., McMullan, R. K., Koetzle, T. F., Lahav, M. & Leiserowitz, L. (1989). *J. Am. Chem. Soc.* **111**, 1035–1040.

Wilkinson, C., Cowan, J. A., Myles, D. A. A., Cipriani, F. & McIntyre, G. J. (2002). *Neutron News*, **13**, 37–41.

Wilkinson, C., Khamis, H. W., Stansfield, R. F. D. & McIntyre, G. J. (1988). *J. Appl. Cryst.* **21**, 471–478.

Wilson, C. C., Myles, D., Ghosh, M., Johnson, L. N. & Wang, W. (2005). *New J. Chem.* **29**, 1318–1322.

Wlodawer, A. & Hendrickson, W. A. (1982). *Acta Cryst.* A**38**, 239–247.

Wolff, S. K., Grimwood, D. J., McKinnon, J. J., Turner, M. J., Jayatilaka, D. & Spackman, M. A. (2012). *CrystalExplorer*, Version 3.1. University of Western Australia, Australia.